energies

MDPI

Article

Numerical Investigation of the Initial Charging Process of the Liquid Hydrogen Tank for Vehicles

Daehoon Kang [1], Sungho Yun [2,*], Bo-kyong Kim [1], Jaewon Kim [1], Gildong Kim [1], Hyunbae Lee [3] and Sangyeol Choi [3]

[1] Smart Electrical & Signaling Division, Korea Railroad Research Institute, Uiwang 16105, Republic of Korea
[2] Railroad Safety Division, Korea Railroad Research Institute, Uiwang 16105, Republic of Korea
[3] Tae Sung S&E, Seoul 18469, Republic of Korea
* Correspondence: hadogo@krri.re.kr

Abstract: Liquid hydrogen has been studied for use in vehicles. However, during the charging process, liquid hydrogen is lost as gas. Therefore, it is necessary to estimate and reduce this loss and simulate the charging process. In this study, the initial charging process of a vehicle liquid hydrogen tank under room temperature and atmospheric pressure conditions was numerically investigated. A transient thermal-fluid simulation with a phase-change model was performed to analyze variations in the volume, pressure, mass flow rate, and temperature. The results showed that the process could be divided into three stages. In the first stage, liquid hydrogen was actively vaporized at the inner wall surface of the storage tank. The pressure increased rapidly, and liquid droplets were discharged into the vent pipe during the second stage. In the third stage, the mass flow rates of liquid and hydrogen gas at the outlet showed significant fluctuations, owing to complex momentum generated by the evaporation and charging flow. The temperatures of the inner and outer walls, and insulation layer, decreased significantly slower than that of the gas region because of its high heat capacity and insulation effect. The optimal structure should be further studied because the vortex, stagnation, and non-uniform cooling of the wall occurred near the inlet and outlet pipes.

Keywords: liquid hydrogen; insulation; charging; filling; CFD; phase-change model

Citation: Kang, D.; Yun, S.; Kim, B.-k.; Kim, J.; Kim, G.; Lee, H.; Choi, S. Numerical Investigation of the Initial Charging Process of the Liquid Hydrogen Tank for Vehicles. *Energies* **2023**, *16*, 38. https://doi.org/10.3390/en16010038

Academic Editor: Attilio Converti

Received: 13 October 2022
Revised: 3 November 2022
Accepted: 15 December 2022
Published: 21 December 2022

1. Introduction

Vehicles substitute their energy storage systems (ESS) with fossil fuels. Hydrogen is lighter in weight even when carrying a larger amount capacity of energy than batteries [1]. Therefore, small vehicles use batteries, whereas large vehicles such as trucks, buses, trains, vessels, and aircraft use hydrogen. Liquid hydrogen is preferred, as it reduces volume. The same volume can carry twice as much energy as high-pressure gaseous hydrogen, at a pressure of 700 bar. In addition, liquid hydrogen uses 30 times less energy than gaseous hydrogen does during charging [2].

Liquid hydrogen research has grown since the 'space race' in 1957; however, it had a long period of stagnation after the last BMW Hydrogen 7 model was produced in 2007. However, after the special report of the Intergovernmental Panel on Climate Change (IPCC) in 2018, research on liquid hydrogen as a fuel source was revived. These institutes form consortia or projects which research the storage of liquid hydrogen. In the aircraft industry, US companies led by Boeing established cryogenic high-efficiency electrical technologies for aircraft (CHEETA) in 2019 [3], and European companies led by Airbus established H2GEAR/H2JET in 2022. Mangold et al. explored the applicability of liquid hydrogen in aircraft. [4] In the shipping industry, Japan established the Hydrogen Energy Supply-chain Technology Research Association (HySTRA) in 2016 [5], and European companies established SEASHUTTLE in 2022. In the train industry, the Korea Railroad Research Institute has been researching liquid hydrogen for the first time [1]. Major research institutes are summarized in Table 1.

Table 1. Major institutes researching liquid hydrogen.

Nations	Major Private Institutes	Major Public Institutes
USA	Chart Industries, Air Products, Boeing, Plug Power, GenH2, Fuel Cell Energy, Bloom Energy, Nikola, Dow, and Cummins.	National Aeronautics and Space Administration (NASA).
EU, UK	Linde, Air Liquide, Shell, Airbus, BMW, Daimler (Mercedez-Benz), HySiLabs, and MAN Energy Solutions.	UK Aerospace Technology Institute (ATI), German Federal Institute for Materials Research and Testing (BAM), and German Aerospace Center (DLR).
Japan	Kawasaki, Iwatani, Toyota.	Japan Aerospace Exploration Agency (JAXA), and New Energy and Industrial Technology Development Organization (NEDO)
Korea	Hyundai, Doosan, Hylium, Blue H2, Parity, Chemical firms (SK, GS, Hyosung, POSCO), and Ship builders including Hyundai, Daewoo, and Samsung.	Korea Institute of Machinery & Materials (KIMM), Korea Electrotechnology Research Institute (KERI), Korea Research Institute of Ships and Ocean Engineering (KRISO), Korea Aerospace Research Institute (KARI), and Korea Railroad Research Institute (KRRI).

Cryogenic liquid hydrogen is lost when a tank is being charged. The loss is more significant at the first filling when the tank is at room temperature. Therefore, the amount of hydrogen lost, and a method for reducing the loss, have been researched.

Various studies on the charging, injection, and pre-cooling processes of liquid hydrogen have been conducted using simulation methods. Tong et al. suggested supercritical hydrogen computational fluid dynamics (CFD) modeling for a spallation neutron source [6], where an optimal jet-to-surface distance of the moderator was suggested. Ma et al. simulated a non-venting charging process under microgravity conditions [7]. The initial high temperature of the wall caused a rapid increase in pressure, but the difference in the final pressure was small. The results showed that pre-cooling could increase the reliability of the system. He et al. calculated the pre-cooling process of a cryogenically compressed hydrogen tank [8]. The cooling time was calculated according to the initial temperature, cooling rate, and pipe diameter, and the optimal design inlet pipe diameter was determined.

The venting, discharging, and pressure control of liquid hydrogen have also been simulated. Adam et al. modeled a 3D-printed tank and verified it using a liquid nitrogen experiment [9]. The weights of the vapor jacket, cryogel, nylon shell, and para-ortho conversion on the thermal effect were calculated. Zheng et al. demonstrated the effects of venting under microgravity [10], using a lumped vapor model, which was verified through 25 orthogonal experiments. The simulation results predicted that the nozzle length and number increased the daily evaporation rate of hydrogen, whereas the diameter had a negligible effect. The authors recommended using two nozzles instead of only one, placed vertically, as it reduces the thermal stratification.

The simultaneous injection and discharge of the cryogenic tank were studied using transient thermal-fluid simulation with a phase-change model because it can implement a phase-change phenomenon due to heat transfer between cryogenic fuel and environmental conditions. Liu et al. suggested a numerical oxygen tank model validated by the experimental results of pressure change over time, in a liquid nitrogen tank [11]. When the mass flow rate of the gas injection increased, the rate of pressure and the final value of vapor condensation increased. Next, they presented numerical 2-dimensional modeling of injecting gas from the top, and discharging liquid from the bottom of the oxygen tank; it was validated through a liquid hydrogen discharge experiment [12,13]. The temperature and phase distributions over time were noted.

In this study, the initial charging process of a liquid hydrogen tank at room temperature and atmospheric pressure was investigated, using a transient thermal-fluid simulation

with a phase-change model. The properties of the hydrogen and storage tank walls were observed during charging.

2. Methodology

2.1. Simulation Domain

Figure 1 shows the simulation schematic of a liquid hydrogen storage tank. To reduce the computation time, owing to rapid phase change, the liquid hydrogen tank was analyzed with 2-dimensional geometry. The structural support was excluded [14]. The inner tank was designed to store approximately 180 L of liquid hydrogen. Its length, height, and thickness were 1530.2, 396.4, and 5 mm, respectively, as shown in Table 2. The diameters of the inlet and outlet pipes were 10.3 mm. The distance between the inlet and the bottom surface of the inner tank was 148.4 mm. Liquid hydrogen tanks are equipped with various thermal insulation technologies to maintain a saturated temperature of 20.4 K at the atmospheric pressure condition [15]. In this study, vacuum insulation, multi-layer insulation (MLI), and foam insulation were used, with widths of 100, 30, and 30 mm, respectively. The outer tank thickness was 5 mm, and the tank material was Stainless Steel 316 L.

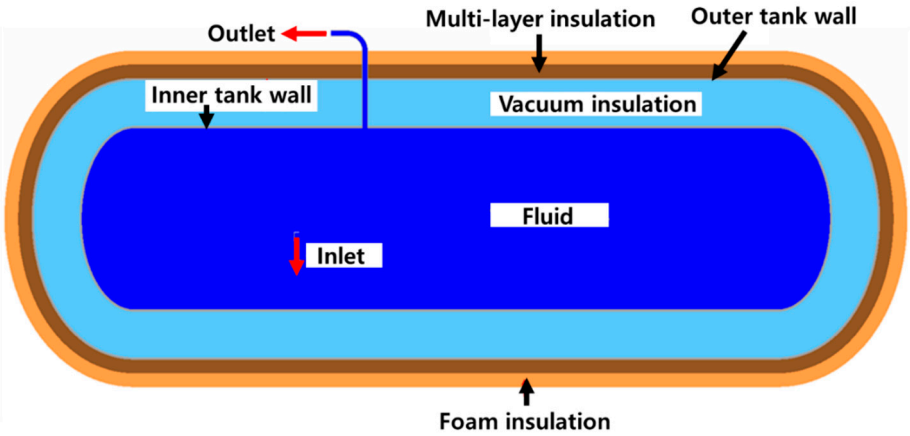

Figure 1. Simulation schematic of the liquid hydrogen storage tank.

Table 2. Specifications of the liquid hydrogen tank.

Parameters	Values
Inner tank length	1530.2 mm
Inner tank height	396.4 mm
Inner tank thickness	5 mm
Diameter of inlet	10.3 mm
Diameter of outlet	10.3 mm
Distance between inlet and bottom surface of inner tank	148.4 mm
Outer tank thickness	5 mm
Vacuum insulation thickness	100 mm
MLI thickness	30 mm
Foam insulation thickness	30 mm

2.2. Simulation Model

The transient thermal fluid simulation with the phase-change model was performed using the ANSYS Fluent 2021 R1 (ANSYS Inc., Canonsburg, PA, USA), which is a high-performance multiphase simulation [16]. The simulation model was developed based on the assumptions below [17].

1. liquid and gas hydrogen were set as incompressible, with constant properties, except for density;
2. density was assumed through the Boussinesq approximation, and
3. helium was set as an ideal gas.

The volume of fluid (VOF) model was used because it includes a multiphase flow tank, in which liquid hydrogen, hydrogen gas, and helium exist in the inner tank. The VOF model is widely used to analyze filling, sloshing, and evaporation in the cryogenic field [13,17]. The governing equations in the simulation are presented as follows [18].

Continuity equation:

$$\frac{\partial}{\partial t}(\alpha_q \rho_q) + \nabla \cdot \left(\alpha_q \rho_q \vec{v}_q\right) = \sum_{p=1}^{n} (\dot{m}_{pq} - \dot{m}_{qp}) \tag{1}$$

$$\frac{\partial \rho V_i}{\partial x_i} = 0 \tag{2}$$

Momentum equation:

$$\frac{\partial}{\partial t}\left(\rho \vec{v}\right) + \nabla \cdot \left(\rho \vec{v} \vec{v}\right) = -\nabla p + \nabla \cdot \left[(\mu + \mu_t)\left(\nabla \vec{v} + \left(\nabla \vec{v}\right)^T\right)\right] + \rho \vec{g} \tag{3}$$

$$\frac{\partial}{\partial x_j}(\rho V_i V_j) = -\frac{\partial p'}{\partial x_i} + \frac{\partial}{\partial x_j}\left[\mu_e\left(\frac{\partial V_i}{\partial x_j} + \frac{\partial V_j}{\partial x_i}\right)\right] \tag{4}$$

Energy equation:

$$\frac{\partial}{\partial t}(\rho E) + \nabla \cdot \left(\vec{v}(\rho E + p)\right) = \nabla \cdot (K \nabla T) + S_h \tag{5}$$

where α, ρ, v, μ, μ_e, and μ_t represent volume fraction, density, velocity, dynamic viscosity, effective viscosity, and eddy viscosity, respectively; g, E, K, T, and S_h represent the gravity, energy term, thermal conductivity, temperature, and energy source term for the product of the mass source respectively; m_{pq} is the mass transfer from p phase to q phase, and m_{qp} is the mass transfer from q phase to p phase.

The turbulence model was applied in the fluid domain because the vaporization of the liquid hydrogen continuously occurred until the temperature inside the tank stabilized, while the liquid hydrogen-filled the tank. The k-epsilon turbulence model was used, which is a type of Reynolds time-averaged Navier-Stokes (RANS) turbulence model, used in all industries [18,19].

$$\frac{\partial}{\partial t}(\rho k) + \nabla \cdot \left(\rho \vec{v} k\right) = \nabla \cdot \left[\left(\mu + \frac{\mu_t}{\sigma_k} \nabla k\right)\right] + G_k + G_b - \rho \varepsilon - Y_M + S_k \tag{6}$$

$$\frac{\partial}{\partial t}(\rho \varepsilon) + \nabla \cdot \left(\rho \vec{v} \varepsilon\right) = \nabla \cdot \left[\left(\mu + \frac{\mu_t}{\sigma_\varepsilon} \nabla \varepsilon\right)\right] + C_{1\varepsilon} \frac{\varepsilon}{k}(G_k + C_{3\varepsilon} G_b) - C_{2\varepsilon} \rho \frac{\varepsilon^2}{k} + S_\varepsilon \tag{7}$$

where k, ε, and S_k denote the turbulence kinetic energy, dissipation rate of the turbulence kinetic energy, and user-defined source term, respectively. G_k, G_b, and Y_M denote the contribution of turbulent kinetic energy owing to the mean velocity, contribution of turbulent kinetic energy owing to the buoyancy, and contribution of the fluctuation dilatation to the overall dissipation rate, respectively. $C_{1\varepsilon}$ and $C_{2\varepsilon}$ are constants, 1.44 and 1.92, respectively. $C_{3\varepsilon}$ is the constant, which is calculated by the ratio of the component of the flow velocity parallel to the gravitational vector and the component of the flow velocity perpendicular to the gravitational vector.

The Lee phase-change model was used to simulate the evaporation of liquid hydrogen. The model has been verified and used as a reasonable phase-change model in the cryogenic field [7,12,13].

$$\frac{\partial}{\partial t}(\alpha_v \rho_v) + \nabla \cdot \left(\alpha_v \rho_v \vec{v}_v\right) = \dot{m}_{l \to v} - \dot{m}_{v \to l} \tag{8}$$

$$\begin{aligned} &\text{If } T_l > T_{sat} \\ &\dot{m}_{l \to v} = r \alpha_l \rho_l (T_l - T_{sat})/T_{sat} \end{aligned} \tag{9}$$

$$\text{If } T_l < T_{sat}$$
$$\dot{m}_{l\to v} = r\alpha_v\rho_v(T_v - T_{sat})/T_{sat} \quad (10)$$

$$S_h = \dot{m}h_{fg} \quad (11)$$

where T_l, T_v, and T_{sat} denote the liquid, vapor, and saturation temperatures, respectively. α and h_{fg} are the volume fraction and latent heat of phase change.

2.3. Boundary Conditions

Table 3 lists the boundary and initial conditions for the simulation. The inlet mass flow rate was chosen as 2 kg·min^{-1} which is the typical charging speed of a gasoline vehicle, and the inlet temperature was chosen as 20 K which the hydrogen can be sufficiently liquid. The environmental conditions were atmospheric pressure (1 atm) and room temperature (293.15 K). The outlet pressure was maintained at 1 atm. The heat transfer coefficient and free stream temperature at the outer surface were 10 W·m^{-2}·K^{-1} and 293.15 K, respectively. The gravity was set in the bottom direction. The initial velocity and temperature were 0 m·s^{-1} and 293.15 K. The liquid hydrogen evaporated at a temperature of 20.4 K while being charged in the tank at room temperature. To prevent contamination, the liquid hydrogen tank was first filled with helium. Figure 2 shows the temperature measurement points used to investigate the local temperatures. The fluid temperatures at the vertical and horizontal points were measured at 45 mm and 150 mm intervals, respectively. Moreover, the tank temperatures of the top and bottom points were measured at 150 mm intervals.

Table 3. Boundary and initial conditions.

Parameters	Values
Boundary conditions	
Mass flow at inlet	0.033 kg·s^{-1} (2 kg·min^{-1})
Temperature at inlet	20 K
Outlet	1 atm
Heat transfer coefficient at outer surface	10 W·m^{-2}·K^{-1}
Free stream temperature at outer surface	293.15 K
Gravity	9.81 m·s^{-2}
Initial conditions	
Initial velocity	0 m·s^{-1}
Initial temperature	293.15 K
Initial gas	Helium 100%

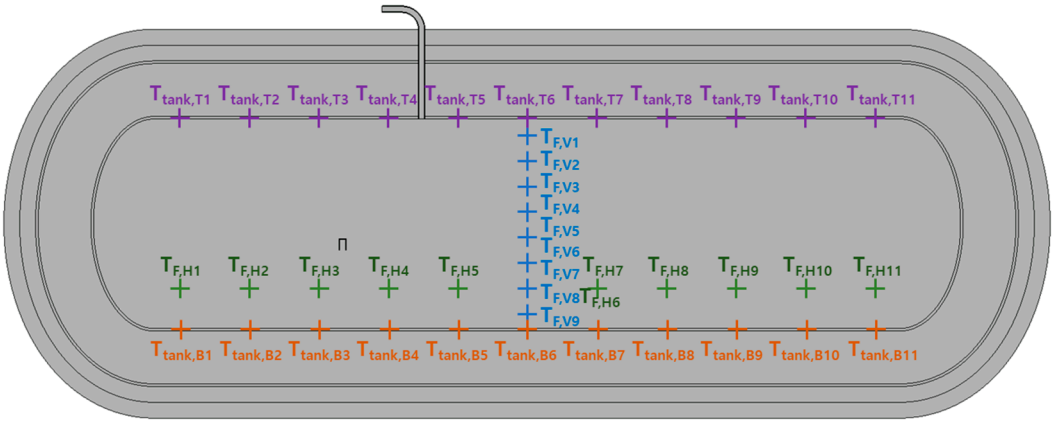

Figure 2. Temperature measurement points.

2.4. Validation

Figure 3 illustrates the grid characteristics of the simulation domains. The grids were generated by the quad-dominant meshing type using ANSYS Meshing 2021 R1 software. A

grid was generated in the fluid domain to which the multiphase model was applied. The four grid types used were 224,286, 429,993, 761,856, and 1,433,386.

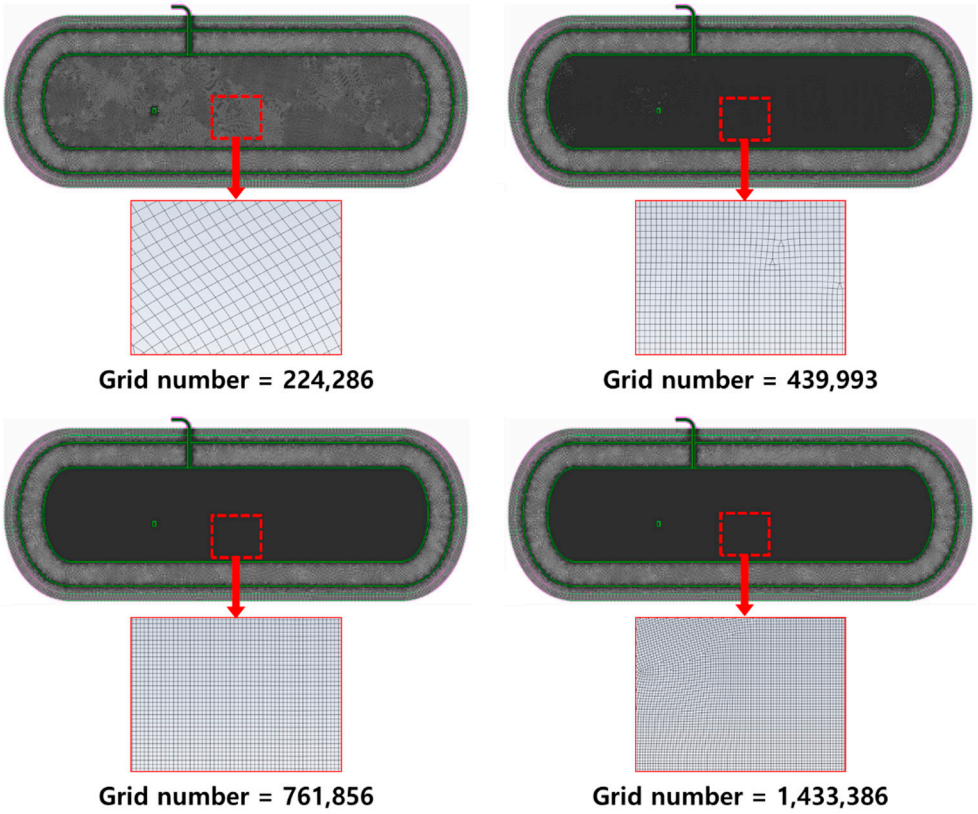

Figure 3. Grid characteristics of simulation domains.

Figure 4 shows the grid-dependency test [20]. During the first 0.1 s, the increasing trend of the volume fraction of liquid hydrogen was little changed, because the phase change had not yet occurred actively. After 0.1 s, the volume fraction of the liquid hydrogen increased rapidly in the grid type of 225,286, and other grid types similarly increased. Therefore, the grid number of 439,993 was selected. This was because its trend of the volume fraction was similar to that of higher grid types, and sufficient grids were generated in the fluid domain where the phase change occurred. Moreover, the grid number of 439,993 was an acceptable quality for the multiphase model because its skewness was <0.48, and its orthogonal quality was >0.5. The time step selected was 1.2×10^{-6} s, because it was confirmed as a condition for convergence, even during rapid phase change. In this study, because the liquid hydrogen evaporated owing to a temperature difference of 253.15 K, a sudden flow characteristic appeared, owing to a very abrupt phase change. During the simulation time of 1.2 s, the physical computation time required was 27 days and 19 h, despite performing 120 parallel processes of Intel Xeon Gold 5115, at 2.4 GHz. Therefore, the initial phenomenon of the filling process was analyzed.

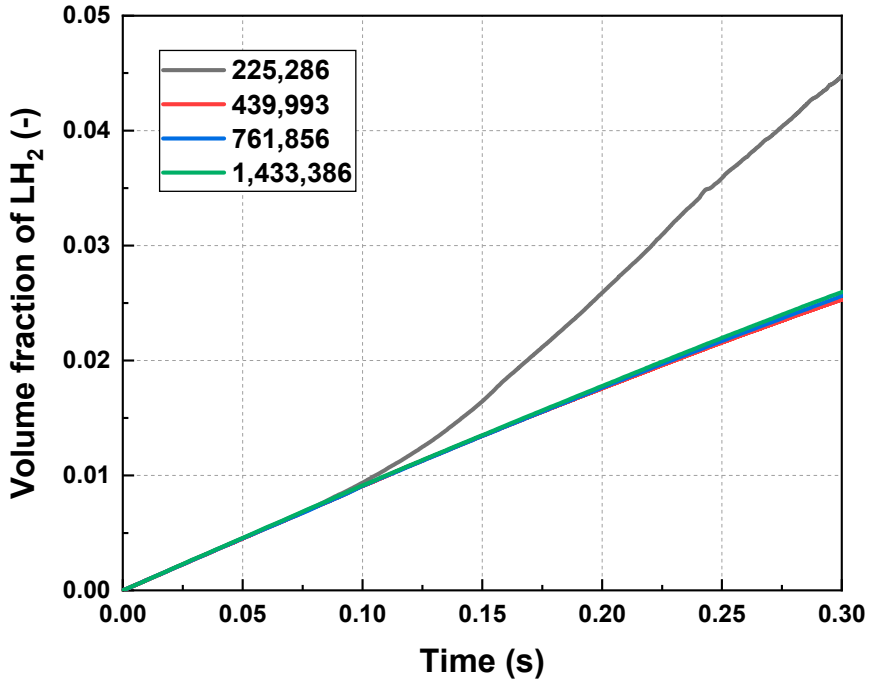

Figure 4. Grid-dependency test.

3. Results and Discussion

3.1. Volume Fraction and Pressure

Figure 5 shows the distribution of the volume fraction of liquid hydrogen according to the charging process. At a time of 0.1 s, the downward stream of liquid hydrogen contacted the bottom of the storage tank, and the stream direction changed from vertical to horizontal. The stream exhibited jet impingement hydrodynamics [21]. Liquid hydrogen with horizontal momentum spread to the left and right in a thin layer, creating a wall jet area on the bottom wall of the storage tank. At 0.2 s, liquid hydrogen was influenced more by the charging momentum than gravity, and it subsequently ascended along the storage tank surface, owing to liquid hydrogen's low density. At 0.3 s, as liquid hydrogen rose to the top of the tank, its flow rate decreased. Moreover, the liquid hydrogen descended and created droplets of various sizes. This was because the dominant force on the liquid hydrogen changed from momentum to gravity. At 0.6 s, the storage tank walls were all wet with liquid hydrogen, and the droplets were distributed inside most of the storage tank. After 0.6 s, some droplets intermittently moved to the outlet along the vent pipe.

Figure 6 depicts the variations in the volume fraction and mass flow rate at the outlet of the liquid hydrogen according to the charging process. At the beginning of charging, the volume fraction of liquid hydrogen increased linearly with the charging time. However, after 0.6 s, as some liquid hydrogen was intermittently discharged through the outlet, the increasing slope of the volume fraction of liquid hydrogen decreased. The flow rate of liquid hydrogen at the outlet fluctuated owing to the influence of the complex momentum generated by the evaporation inside the storage tank.

Figure 7 shows the distribution of the volume fraction of hydrogen gas, according to the charging process and streamline at 0.7 s. At 0.1 s, hydrogen gas was generated from the bottom wall of the tank, as liquid hydrogen rapidly evaporated due to the significant temperature difference of over 273 K between the liquid hydrogen and the tank wall. At the time of 0.2 s and 0.3 s, hydrogen gas was generated on the wall of the storage tank along the movement path of the liquid hydrogen. After 0.4 s, some of the hydrogen gas was discharged to the outlet around the vent pipe owing to its low density. After 0.7 s, hydrogen gas was distributed in all areas of the storage tank. However, as shown in Figure 7b, some helium was trapped on the left and right sides of the center location of the tank, as it was

under the influence of the hydrogen gas vertex. The remaining helium was gradually discharged, along with hydrogen gas, as the internal pressure of the storage tank increased.

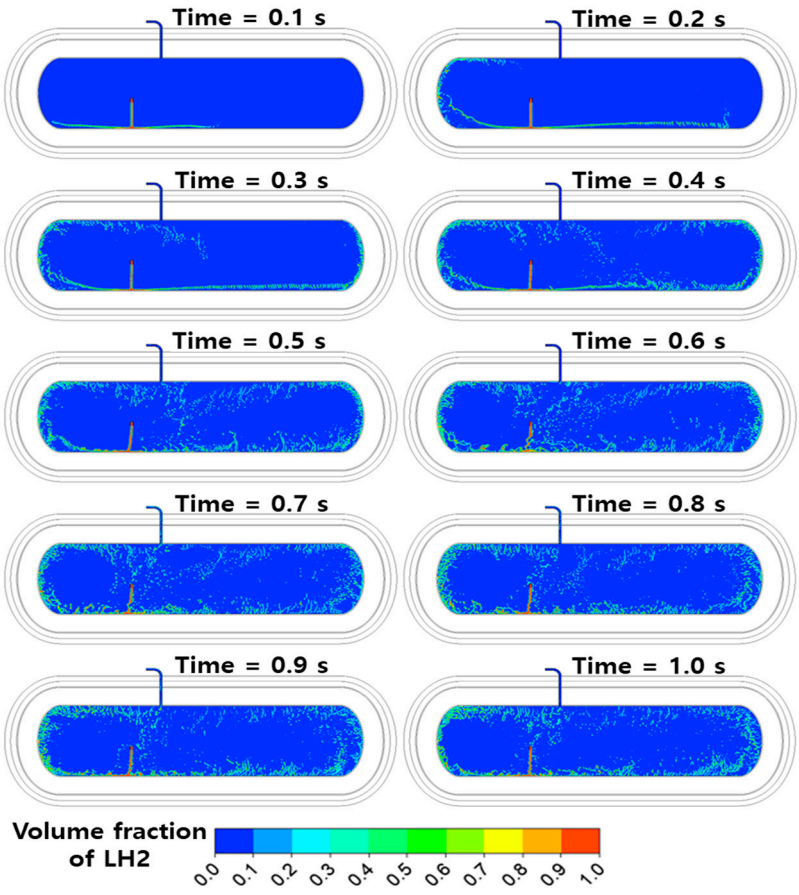

Figure 5. Distributions of volume fraction of liquid hydrogen according to charging process.

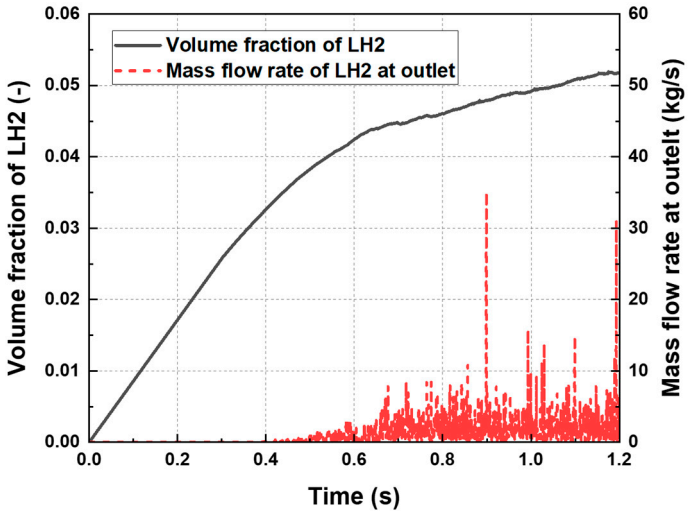

Figure 6. Variation in the volume fraction and mass flow rate at outlet of liquid hydrogen according to charging process.

Figure 8 depicts the variations in the volume fraction and mass flow rate at the outlet, according to the charging process. Helium, which was fully charged in the storage tank under the initial conditions, was moved to the outlet as the liquid hydrogen was supplied into the tank. However, at 0.6 s, the mass flow rate of helium gas at the outlet decreased,

because the helium gas was trapped in the hydrogen gas vortex stream. After 0.8 s, the mass flow rate of helium gas at the outlet increased, owing to the increased pressure of hydrogen gas in the storage tank. After 1.1 s, the mass flow rate of helium gas at the outlet was low, because most of it was discharged from the tank. The gaseous hydrogen exhaust started to increase after 0.3 s. The complex behavior of evaporation caused an extensive variation range in the mass flow rate of hydrogen gas at the outlet, and the highest mass flow rate of hydrogen gas at the outlet occurred at 0.9 s. The mass flow ratio at the outlet was defined as the value obtained by dividing the mass flow rate of hydrogen gas by the total gas mass flow rate at the outlet. After 0.3 s, the mass flow ratio at the outlet increased rapidly (by ~90%) owing to the evaporation effect. At 0.43 s, the mass flow ratio instantaneously decreased by ~60% because helium, which is less dense than hydrogen gas, collected at the top of the storage tank and was briefly discharged. After 0.7 s, the mass flow ratio at the outlet was 96–98% because most of the helium gas had been discharged into the outlet. Finally, at 1.2 s, the mass flow ratio at the outlet reached 97.3% as it was trapped by the hydrogen gas.

Figure 9 shows the variation in the mass fraction in the tank according to the charging process. The hydrogen mass fraction in the tank means the purity of hydrogen because it was defined as the sum of the liquid and gaseous hydrogen mass fraction. During 0.3 s, the hydrogen mass fraction in the tank increased, and the helium mass fraction in the tank decreased rapidly. At 0.3 s, the hydrogen and helium mass fractions in the tank were 90.60% and 9.40%, respectively. After 0.6 s, the slope of the hydrogen and helium mass fraction in the tank was small value because there was less helium remaining in the tank. At 1.2 s, the hydrogen mass fraction in the tank reached 98.77%. Therefore, to satisfy the 99.97% purity of hydrogen in the storage tank (required by the International Organization for Standardization), a significant charge loss was expected to occur [22].

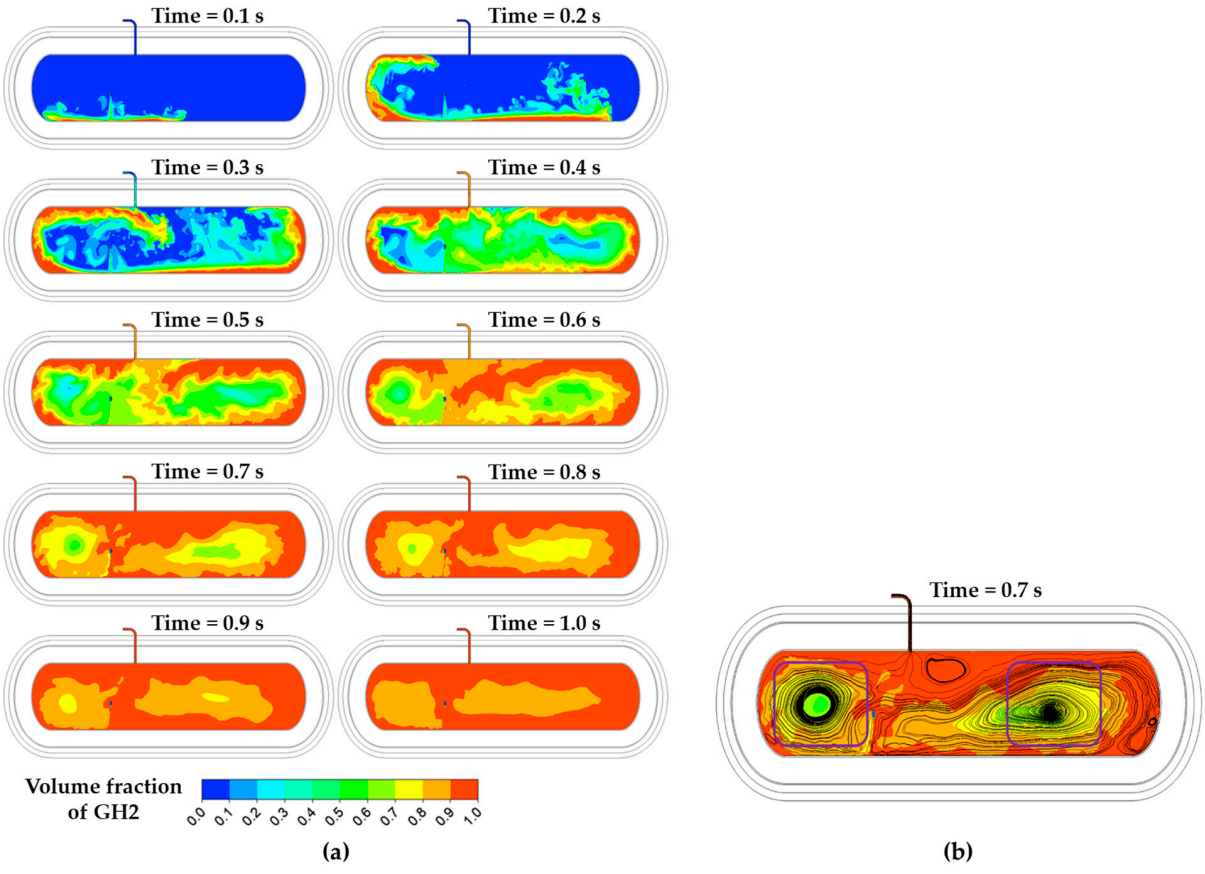

Figure 7. Distributions of the volume fractions of hydrogen gas (**a**) change according to charging process and (**b**) with streamline at 0.7 s.

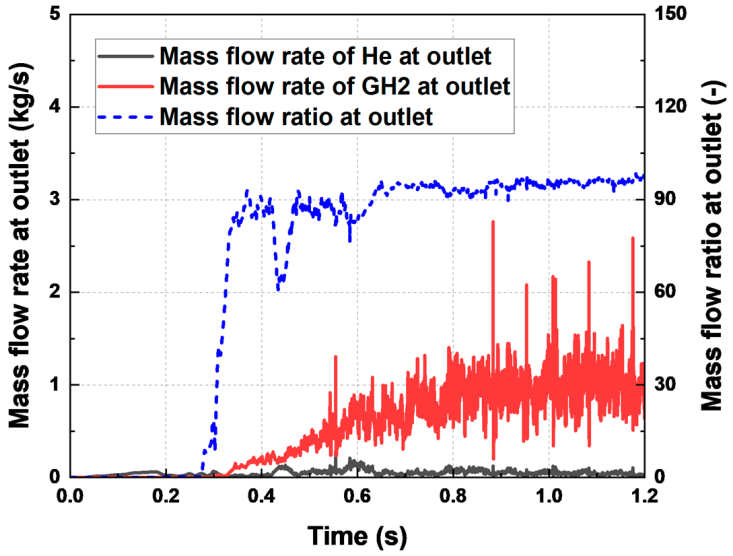

Figure 8. Variations in the volume fraction and mass flow rate at outlet according to charging process.

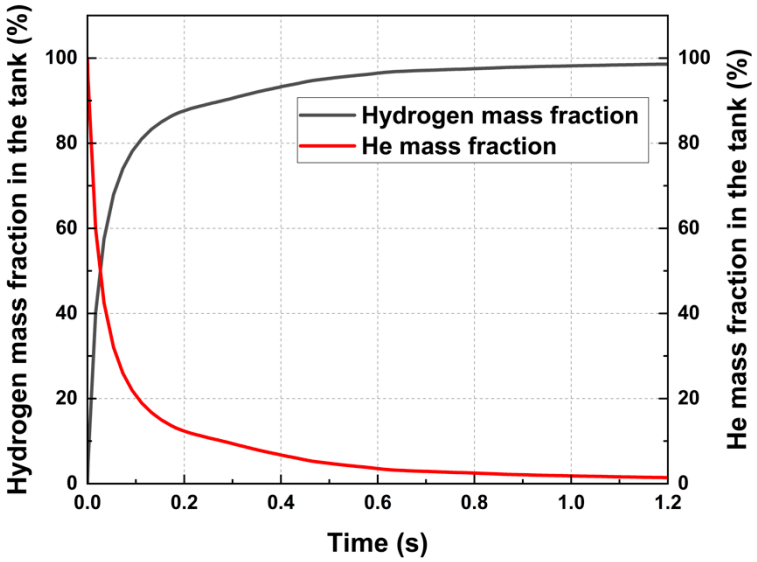

Figure 9. Variation in the mass fraction in the tank according to charging process.

Figure 10 shows the variations in the inner tank pressure. The charging process was divided into three stages based on the variation in the pressure inside the storage tank. In the first stage (up to 0.3 s), there was a negligible pressure change, owing to the small amount of vaporized hydrogen gas. In the second stage (up to 0.9 s), the pressure rapidly increased, because the evaporated hydrogen gas filled the tank. At 0.9 s, the pressure was 50,960 Pa but then decreased since the hydrogen gas was continuity discharged to the outlet as shown in Figure 8. In the third stage, the pressure was balanced (owing to the evaporation of gaseous hydrogen and the discharge), and approached a steady-state condition. During the third stage, the difference between the maximum and minimum pressures was 2962 Pa, and the increase and decrease in pressure were repeated, owing to the fluctuating flow of liquid and gaseous hydrogen in the tank as shown in Figures 5 and 7.

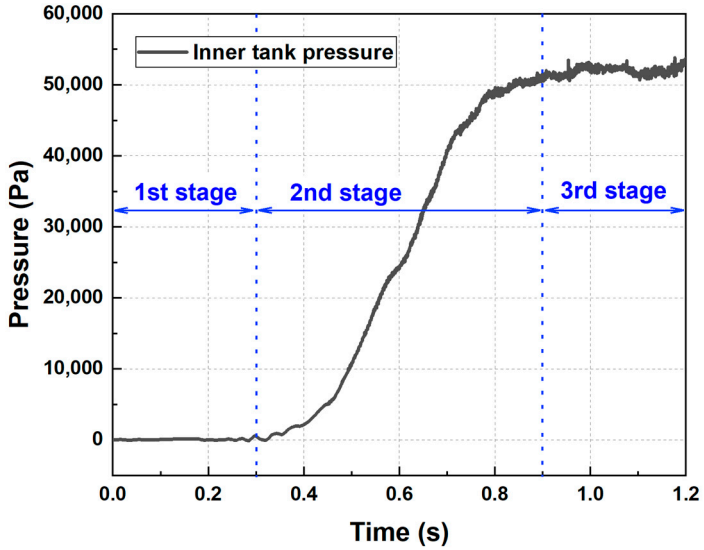

Figure 10. Variation in the inner tank pressure.

3.2. Temperature

Figure 11 shows the temperature distributions according to the charging process. When 20 K of liquid hydrogen was supplied to the storage tank at room temperature, the temperature of the gas region decreased rapidly. The temperature rapidly decreased around the walls of the storage tank, through which the liquid hydrogen flowed. However, convection was promoted by evaporation, and the temperature inside the storage tank quickly reached equilibrium owing to the active heat exchange between the liquid and gas. The temperature of the inner/outer wall and insulation layer showed little change.

Figure 12 shows the variation in the average temperature according to the charging process. Up to a time of 0.4 s, the temperature inside the storage tank decreased rapidly to 47.7 K, due to cryogenic liquid hydrogen and vaporized hydrogen gas. The fluid temperature gradually decreased as the hydrogen gas diffused. At 1.2 s, the fluid temperature decreased to 32.8 K. The outlet temperature decreased sharply after 0.3 s when the liquid hydrogen started to discharge. Thereafter, the outlet temperature gradually decreased as the helium was cooled by the liquid hydrogen, and hydrogen gas was discharged. The inner and outer walls of the storage tank showed very small temperature changes owing to their high heat capacity and insulation effect. The inner and outer wall temperatures decreased by 11.5 K and 0.04 K, respectively, during 1.2 s. The reduction in temperature of the outer tank wall was particularly small because there was a vacuum insulation layer between the inner and outer tank walls.

Figure 12 shows the necessity of the pre-cooling process before liquid hydrogen filling. The fluid temperature inside the storage tank decreased significantly; additionally, the temperature of the inner and outer tank walls showed a very large temperature difference from the liquid-hydrogen temperature. There are various candidates for pre-cooling materials; however, refrigerants, liquid hydrogen, and liquid nitrogen are recommended as pre-cooling materials because they are relatively inexpensive and have low environmental pollution effects. If pre-cooling using liquid nitrogen at approximately 77 K is performed, liquid hydrogen for cooling the storage tank can be saved.

Figure 13 shows the variations in the vertical and horizontal fluid temperatures according to the charging process. As shown in Figure 13a, only $T_{F,V8}$ and $T_{F,V9}$ (located at the bottom of the storage tank) decreased in temperature, as the liquid hydrogen was charged up to 0.3 s. However, all vertical fluid temperatures decreased rapidly between 0.3 and 0.6 s, as liquid hydrogen was vaporized, and hydrogen gas was diffused. Subsequently, all the vertical fluid temperatures gradually decreased, and therefore, the temperature difference in the vertical direction also decreased.

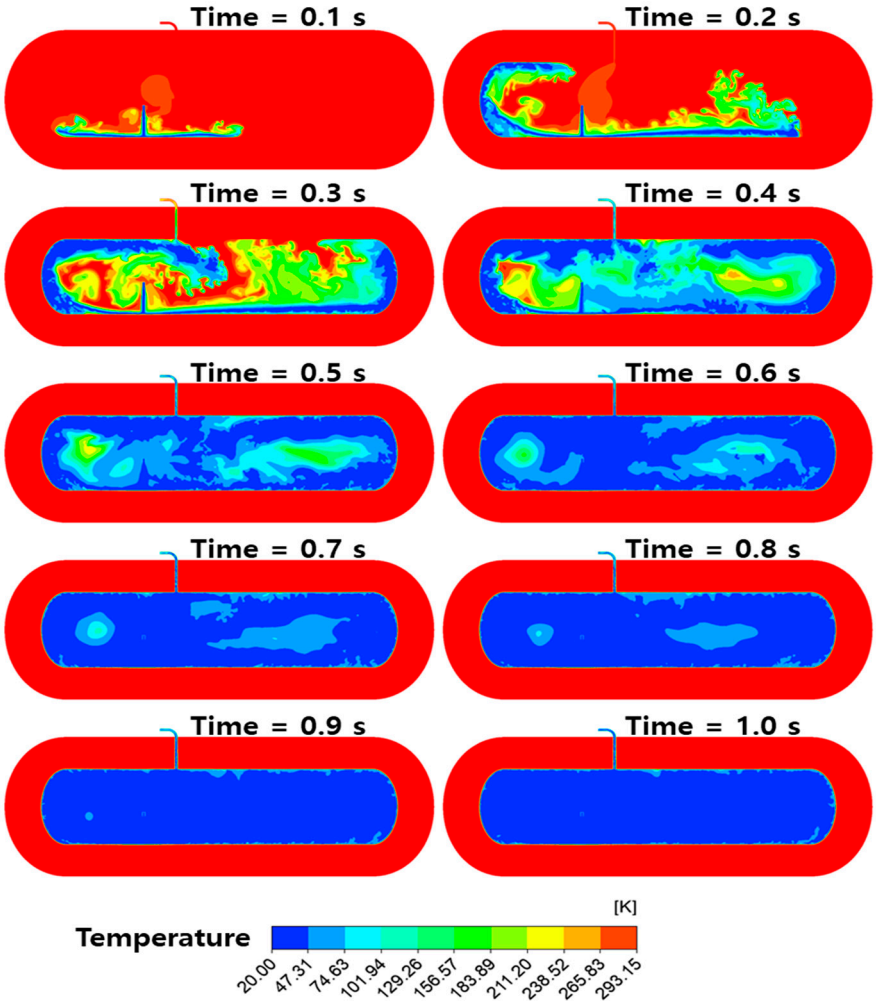

Figure 11. Distributions of temperature according to charging process.

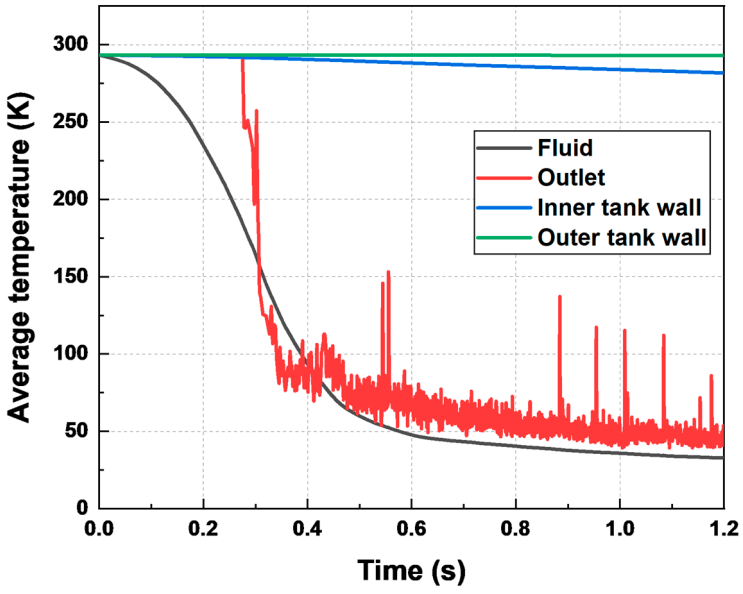

Figure 12. Variation in the average temperatures according to charging process.

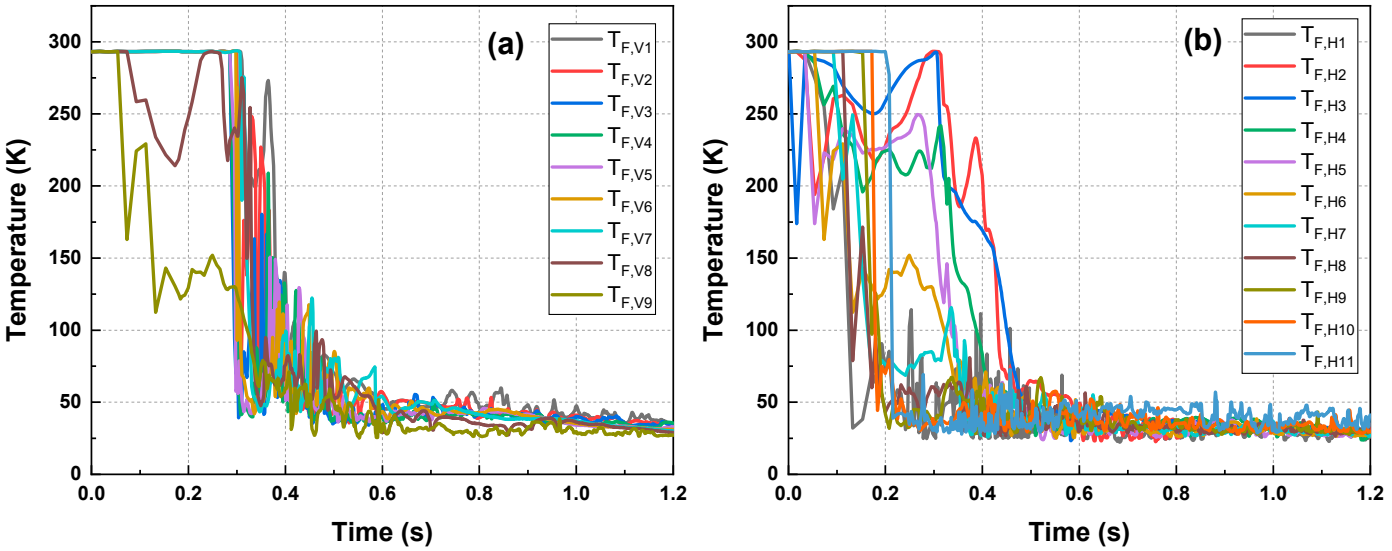

Figure 13. Variations in (**a**) the vertical fluid temperature and (**b**) horizontal fluid temperature according to charging process.

As shown in Figure 13b, the horizontal fluid temperature distribution decreased more slowly than the vertical temperature distribution at some temperatures. Specifically, $T_{F,H3}$ and $T_{F,H4}$ decreased rapidly after 0.4 s, despite being near the inlet. As shown in Figure 14, the liquid hydrogen flow, in the form of jet impingement falling vertically from the inlet, forms a thin liquid hydrogen film on the wall after colliding with the bottom of the tank. Therefore, the two points were slowly immersed in liquid hydrogen, and the temperature decreased slowly compared with the other horizontal flow temperatures.

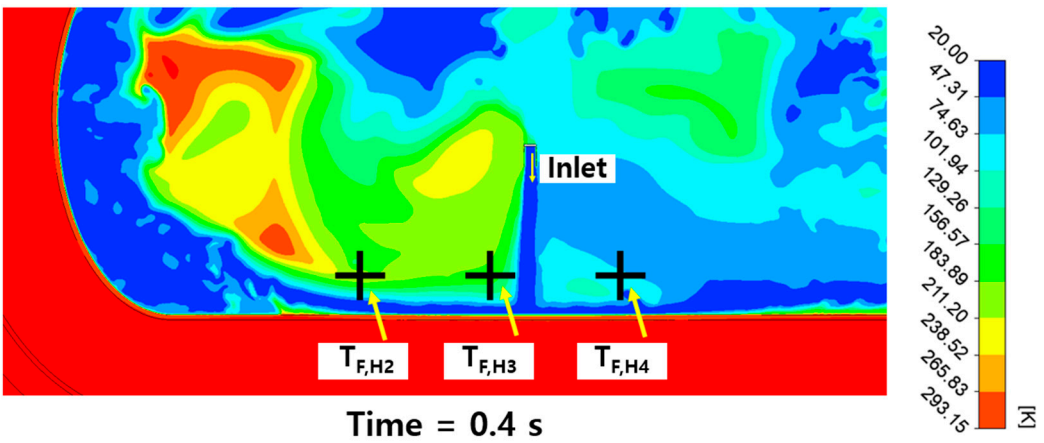

Figure 14. Distributions of the temperature at the horizontal temperature points of 2, 3, and 4.

Figure 15 depicts the variations in the top and bottom tank temperatures according to the charging process. As shown in Figure 15a, all temperatures at the top of the tank started to decrease after 0.3 s. The external tank temperature located at the top of the tank ($T_{Tank,T1}$ and $T_{Tank,T11}$) decreased rapidly, compared to other temperatures, as they were the first to have contact with the liquid hydrogen rising up to the tank surface, as shown in Figure 5. However, the temperatures at the top of the tank (close to the outlet) decreased very slowly owing to sufficient heat exchange with vaporized gaseous hydrogen. The maximum temperature difference between the top of the tank for 1.2 s was 16.3 K.

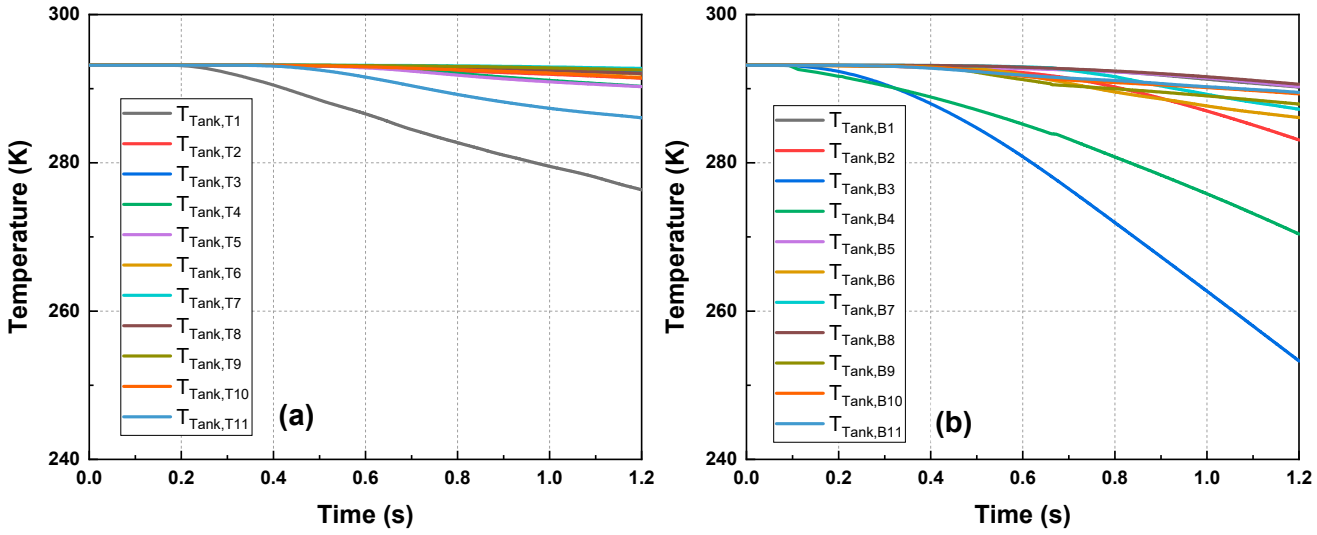

Figure 15. Variations in tank temperature according to charging process for (**a**) the top of the tank, and (**b**) the bottom of the tank.

As shown in Figure 15b, all temperatures at the bottom of the tank started to decrease after 0.3 s except $T_{Tank,B3}$, and $T_{Tank,B4}$. The temperatures of the two points decreased rapidly after 0.1 s because they were in the stagnated regions, where the jet-impinged liquid hydrogen from the inlet was in direct contact with the tank wall. During the simulation, $T_{Tank,B3}$ exhibited the greatest decrease in temperature, which was 19.9 K. As shown in Figure 16, the temperatures of the two points decreased to the temperature inside the tank wall, owing to the continuous jet impingement effect. However, the temperature of the other tank wall did not sufficiently cool, as the two points had. Therefore, additional research is required to reduce the charging time and energy consumption by sufficiently reducing the temperature of the storage tank through the pre-cooling process.

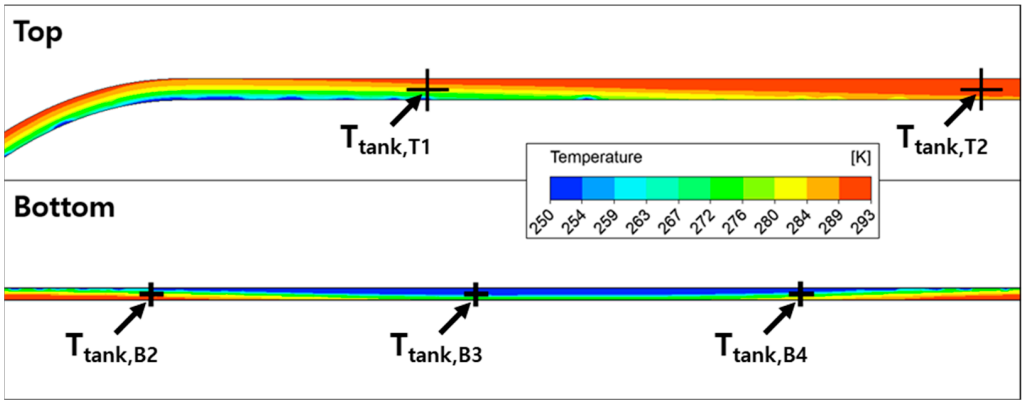

Figure 16. Distributions of the temperature at the top and bottom of the tank.

4. Conclusions

In this study, the initial charging process of a liquid hydrogen tank was investigated using a transient thermal-fluid simulation with a phase-change model. Using this model, which was validated by grid-dependency tests, variations in the volume fraction, pressure, mass flow rate, and temperature were investigated during the charging process. The initial conditions of the tank are filled with 20 K helium. Moreover, the initial tank temperature and outlet pressure were set to 293.15 K and 1 atm.

After 0.6 s, all the storage tank walls were wet with liquid hydrogen, and some liquid hydrogen droplets intermittently moved toward the outlet because of the active evaporation of liquid hydrogen. During the time of 1.2 s, the mass flow ratio at the outlet was 97.3%, as

it was trapped by the hydrogen gas. The mass flow rates of liquid and gaseous hydrogen fluctuated significantly, owing to the influence of the complex momentum generated by the evaporation and charging flow. Additionally, the charging process was divided into three stages based on the variation in the pressure inside the storage tank. Time indicators to divide the stages occurred at 0.4 s and 0.9 s, based on the pressure increasing rate. Moreover, at 1.2 s, the temperatures of the fluid, inner wall, and outer wall decreased by 260.3, 11.5, and 0.04 K, respectively. Therefore, the decreasing rates of the temperatures of the inner and outer walls were significantly lower than that of the fluid, owing to its high heat capacity and insulation effect.

Author Contributions: Conceptualization, D.K. and S.Y.; methodology, S.Y., B.-k.K. and J.K.; software, H.L. and S.C.; validation, H.L. and S.C.; formal analysis, H.L. and S.C.; investigation, D.K. and S.Y.; resources, G.K.; writing—original draft preparation, D.K. and S.Y.; writing—review and editing, D.K., S.Y. and G.K.; supervision, S.Y. and G.K.; project administration, G.K., B.-k.K. and J.K.; funding acquisition, G.K. All authors have read and agreed to the published version of the manuscript.

Funding: This research was funded by a grant from the R&D program (PK2203F1) of the Korea Railroad Research Institute (KRRI).

Conflicts of Interest: The authors declare no conflict of interest.

References

1. Kang, D.; Yun, S.; Kim, B.-K. Review of the Liquid Hydrogen Storage Tank and Insulation System for the High-Power Locomotive. *Energies* **2022**, *15*, 4357. [CrossRef]
2. Simon, S.; Steffen, M. Technology Pitch: Subcooled Liquid Hydrogen (sLH2). In Proceedings of the NOW & CEP Heavy Duty Event, Virtual Conference, 21 April 2021. Available online: https://www.now-gmbh.de/wp-content/uploads/2021/05/Heavy-Duty-Event-Subcooled-Liquid-Hydrogen-sLH2-Schaefer-Linde-Maus-Daimler.pdf (accessed on 15 December 2022).
3. Telikapalli, S.; Swain, R.M.; Cheetham, P.; Kim, C.H.; Pamidi, S.V. Electric Aircraft Fueled by Liquid Hydrogen and Liquefied Natural Gas. In *Advances in Cryogenic Engineering—Materials: Proceedings of the International Cryogenic Materials Conference (ICMC), Virtual Conference, USA, 19–23 July 2021*; IOP Science: Bristol, UK, 2021. [CrossRef]
4. Mangold, J.; Silberhorn, D.; Moebs, N.; Dzikus, N.; Hoelzen, J.; Zill, T.; Strohmayer, A. Refueling of LH2 Aircraft—Assessment of Turnaround Procedures and Aircraft Design Implication. *Energies* **2022**, *15*, 2475. [CrossRef]
5. Ring, T. HySTRA developing green hydrogen supply chain tech in Japan. *Fuel Cells Bull.* **2019**, *2019*, 10–11. [CrossRef]
6. Tong, J.; Zhu, L.; Lu, Y.; Liang, T.; Lu, Y.; Wang, S.; Yu, C.; Dong, S.; Tan, H. Study of Flow and Heat Transfer for the Supercritical Hydrogen in Spallation-Type Cylindrical Neutron Moderator. *Energies* **2021**, *14*, 5856. [CrossRef]
7. Ma, Y.; Li, Y.; Zhu, K.; Wang, Y.; Wang, L.; Tan, H. Investigation on no-vent filling process of liquid hydrogen tank under microgravity condition. *Int. J. Hydrogen Energy* **2017**, *42*, 8264–8277. [CrossRef]
8. He, M.; Lv, C.; Gong, L.; Wu, J.; Zhu, W.; Zhang, Y.; Zhang, M.; Sun, W.; Sha, L. The design and optimization of a cryogenic compressed hydrogen refueling process. *Int. J. Hydrogen Energy* **2021**, *46*, 29391–29399. [CrossRef]
9. Adam, P.; Leachman, J.; Shoemake, E. Computational Fluid Dynamics Model of a 3D Printed Liquid Hydrogen Tank with Vapor Cooled Shielding for Use in Unmanned Aerial Vehicles. In Proceedings of the Cryogenic Engineering Conference (CEC)—International Cryogenic Materials Conference (ICMC), Madison, WI, USA, 11 July 2017. Available online: https://indico.cern.ch/event/578092/contributions/2538308/attachments/1490141/2315895/CEC2017.pdf (accessed on 15 December 2022).
10. Zheng, Y.; Yang, P.; Liu, Y.; Yang, Q.; Yan, C.; Wang, X. Parametric optimization and analysis of thermodynamic venting system in liquid hydrogen tank under microgravity. *Int. J. Hydrogen Energy* **2021**, *46*, 40041–40053. [CrossRef]
11. Liu, Z.; Yang, Y.; Liu, Y.; Li, Y. Effect of gas injection mass flow rates on the thermal behavior in a cryogenic fuel storage tank. *Int. J. Hydrogen Energy* **2022**, *47*, 14703–14713. [CrossRef]
12. Liu, Z.; Yin, X.; Liu, Y.; Li, Y. Investigation on Thermal Behavior During Pressurization Discharge of Liquid Oxygen under Different Acceleration Levels. *Microgravity Sci. Technol.* **2022**, *34*, 27. [CrossRef]
13. Liu, Z.; Pan, H.; Liu, Y.; Li, Y. Thermodynamic performance on the pressurized discharge process from a cryogenic fuel storage tank. *Int. J. Hydrogen Energy* **2022**, *47*, 12107–12118. [CrossRef]
14. Jiang, W.; Sun, P.; Li, P.; Zuo, Z.; Huang, Y. Transient thermal behavior of multi-layer insulation coupled with vapor cooled shield used for liquid hydrogen storage tank. *Energy* **2021**, *231*, 120859. [CrossRef]
15. Wang, P.; Ji, L.; Yuan, J.; An, Z.; Yan, K.; Zhang, J. The influence of inner material with different average thermal conductivity on the performance of whole insulation system for liquid hydrogen on orbit storage. *Int. J. Hydrogen Energy* **2021**, *46*, 10913–10923. [CrossRef]
16. Wu, S.; Ju, Y. Numerical study of the boil-off gas (BOG) generation characteristics in a type C independent liquefied natural gas (LNG) tank under sloshing excitation. *Energy* **2021**, *223*, 120001. [CrossRef]

17. Liu, Z.; Feng, Y.; Liu, Y.; Lei, G.; Li, Y. Fluid sloshing dynamic performance in a fuel storage tank under sinusoidal excitations. *Appl. Therm. Eng.* **2020**, *168*, 114814. [CrossRef]
18. *UDF Manual, ANSYS FLUENT Theory Guide*; ANSYS, Inc.: Canonsburg, PA, USA, 2011; 794p.
19. Yun, S.; Hong, S.H.; Song, K.S.; Kwon, J.; Kim, Y. Experimental and numerical analyses of quenching performance of hot stamping blanks by two-phase refrigerant cooling using R1234yf. *Int. J. Heat Mass Transf.* **2021**, *173*, 121231. [CrossRef]
20. Yun, S.; Kim, J. Numerical Evaluation of a Novel Vertical Drop Airflow System to Mitigate Droplet Transmission in Trains. *Atmosphere* **2022**, *13*, 829. [CrossRef]
21. Hussain, L.; Khan, M.M.; Masud, M.; Ahmed, F.; Rehman, Z.; Amanowicz, Ł.; Rajski, K. Heat Transfer Augmentation through Different Jet Impingement Techniques: A State-of-the-Art Review. *Energies* **2021**, *14*, 6458. [CrossRef]
22. *ISO 14687:2019*; Hydrogen Fuel Quality—Product Specification. International Organization for Standardization: Geneva, Switzerland, 2019.